

Environmental effect on the subhalo abundance — a solution to the missing dwarf problem.

Tomoaki ISHIYAMA

*National Astronomical Observatory, Mitaka, Tokyo 181-8588, Japan
and Department of General System Studies, College of Arts and Sciences,
University of Tokyo, Tokyo 153-8902, Japan*

ishiyama@cfca.jp

Toshiyuki FUKUSHIGE

K&F Computing Research Co., Chofu, Tokyo 192-0026, Japan

fukushig@kfcr.jp

and

Junichiro MAKINO

National Astronomical Observatory, Mitaka, Tokyo 181-8588, Japan

makino@cfca.jp

(Received ; accepted)

Abstract

Recent high-resolution simulations of the formation of dark-matter halos have shown that the distribution of subhalos is scale-free, in the sense that if scaled by the velocity dispersion of the parent halo, the subhalo velocity distribution function of galaxy-sized and cluster-sized halos are identical. For cluster-sized halos, simulation results agreed well with observations. Simulations, however, predicted far too many subhalos for galaxy-sized halos. Our galaxy has several tens of known dwarf galaxies. On the other hands, simulated dark-matter halos contain thousands of subhalos. We have performed simulation of a single large volume and measured the abundance of subhalos in all massive halos. We found that the variation of the subhalo abundance is very large, and those with largest number of subhalos correspond to simulated halos in previous studies. The subhalo abundance depends strongly on the local density of the background. Halos in high-density regions contain large number of subhalos. Our galaxy is in the low-density region. For our simulated halos in low-density regions, the number of subhalos is within a factor of four to that of our galaxy. We argue that the “missing dwarf problem” is not a real problem but caused by the biased selection of the initial conditions in previous studies, which were not appropriate for field galaxies.

Key words: cosmology: theory—galaxies: dwarf— methods: n-body simulations

1. Introduction

Klypin et al. (1999) and Moore et al.(1999a) analyzed the structure of dark-matter halos formed in their high-resolution cosmological N -body simulations and found that dark matter halos of the mass comparable to the Local group contain far too many subhalos compared to known dwarf galaxies in the Local group. This “missing dwarf problem” was confirmed by many simulations based on the concordance cosmological model, and has been regarded as one of its most serious problems. A number of “solutions” have been proposed, including “warm” dark matter (Kamionkowski, Liddle 2000), self-interacting dark matter (Spergel, Steinhardt 2000), suppression of star formation by early reionization (Susa, Umemura 2004), self-regulation of star formation in small halos (Stoehr et al. 2002; Kravtsov et al. 2004), but none is widely accepted as a clear-cut solution.

In this paper, we study the environmental effect on the subhalo abundance. In almost all previous studies of substructures in the dark-matter halos, simulations are done following the “re-simulation” prescription, in which one

first simulates a fairly large volume (for galaxy-sized halos typically a 50-100Mpc cube) with low mass resolution and identifies the candidate regions to perform high-resolution simulations. Then, one makes the same initial model, but with higher mass resolution for the candidate regions, and analyze the result. Clearly, this is not the way to obtain an unbiased sample of dark-matter halos.

In order to see if the bias has any effect, we simulated a relatively small region (a 21.4 Mpc box) with high mass resolution (mass of particles = $3 \times 10^6 M_\odot$) and high spacial resolution (softening length= 1.8kpc). Number of particles used is 512^3 . Simulation was performed with TreePM code (Yoshikawa, Fukushige 2005) on a 12-node GRAPE-6A cluster (Sugimoto, et al. 1990; Fukushige et al. 2005). Since the simulated region is still relatively small, we might be affected from the bias due to the fact we neglected the contributions of fluctuations with the wavelength longer than the vbox size, but we are free from the halo-selection bias, since we analyzed all halos with rotation velocity larger than 200 km/s. There are 21 such halos and we give them ID numbers in order of their masses.

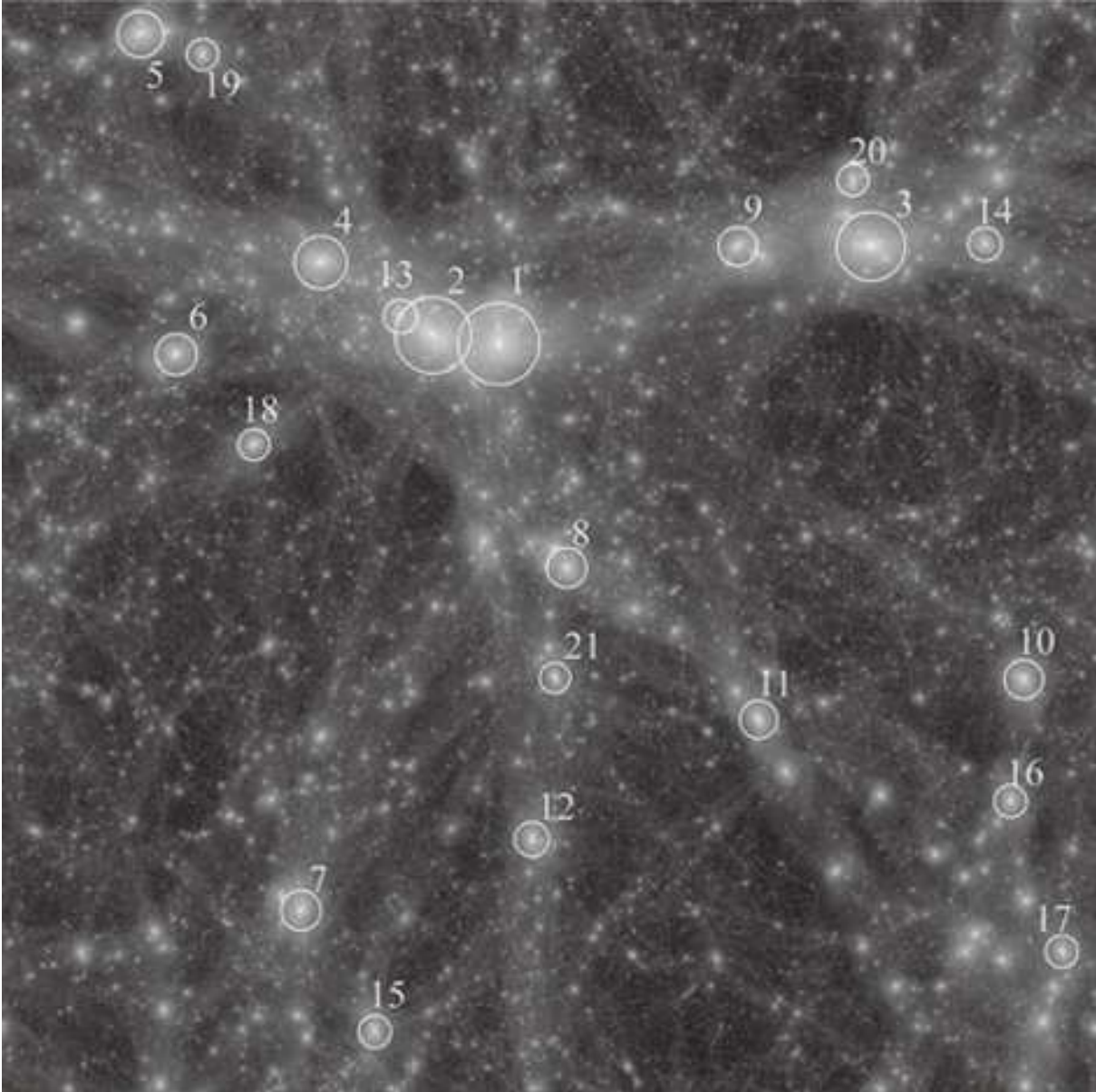


Fig. 1. Snapshot of the simulation box whose size is 21.4Mpc at $z = 0$. The circles shows the virial radii of the 21 selected halos. The numbers near circles indicate the halo IDs.

The structure of this paper is as follows. In section 2, we describe the method of our N -body simulation. In section 3, we present the results of simulation. Section 4 is for conclusion.

2. Method

We performed an LCDM ($\Omega_0 = 0.3$, $\lambda_0 = 0.7$, $h = 0.7$, $\sigma_8 = 1.0$) cosmological simulations. Here, Ω_0 is the density parameter, λ_0 is the dimensionless cosmological constant, $H_0 = 100h \text{ km/s} \cdot \text{Mpc}^{-1}$ at the present epoch, and σ_8 is the top-hat filtered mass variance at $8h^{-1} \text{ Mpc}$. The initial particle distribution was generated using GRAFIC1 code (Bertschinger 1995).

We followed the evolution of 512^3 particles with masses of $3 \times 10^6 M_\odot$ in a comoving 21.4 Mpc cube, using a

parallel TreePM code (Yoshikawa, Fukushige 2005) on a GRAPE-6A cluster (Fukushige, Makino, Kawai 2005). We set the grid size for the PM part as 256^3 , and the opening parameter for the tree part as $\theta = 0.5$.

We integrated the system in the comoving coordinates with a leap-frog integrator with shared timestep. The step size is adaptive and determined according to $\min(2.0\sqrt{\varepsilon/|\vec{a}_i|}, 2.0\varepsilon/|\vec{v}_i|)$. We integrated the system from $z = 84$ to 0 and the total number of timesteps was 4930. The (Plummer) gravitational softening we used is constant in the comoving coordinate upto $z = 10$, and is constant (1.8 kpc) in the physical coordinate from $z = 10$ to $z = 0$.

We used a 12-node GRAPE-6A cluster at University of Tokyo. The parallel cluster consists of 12 host computers

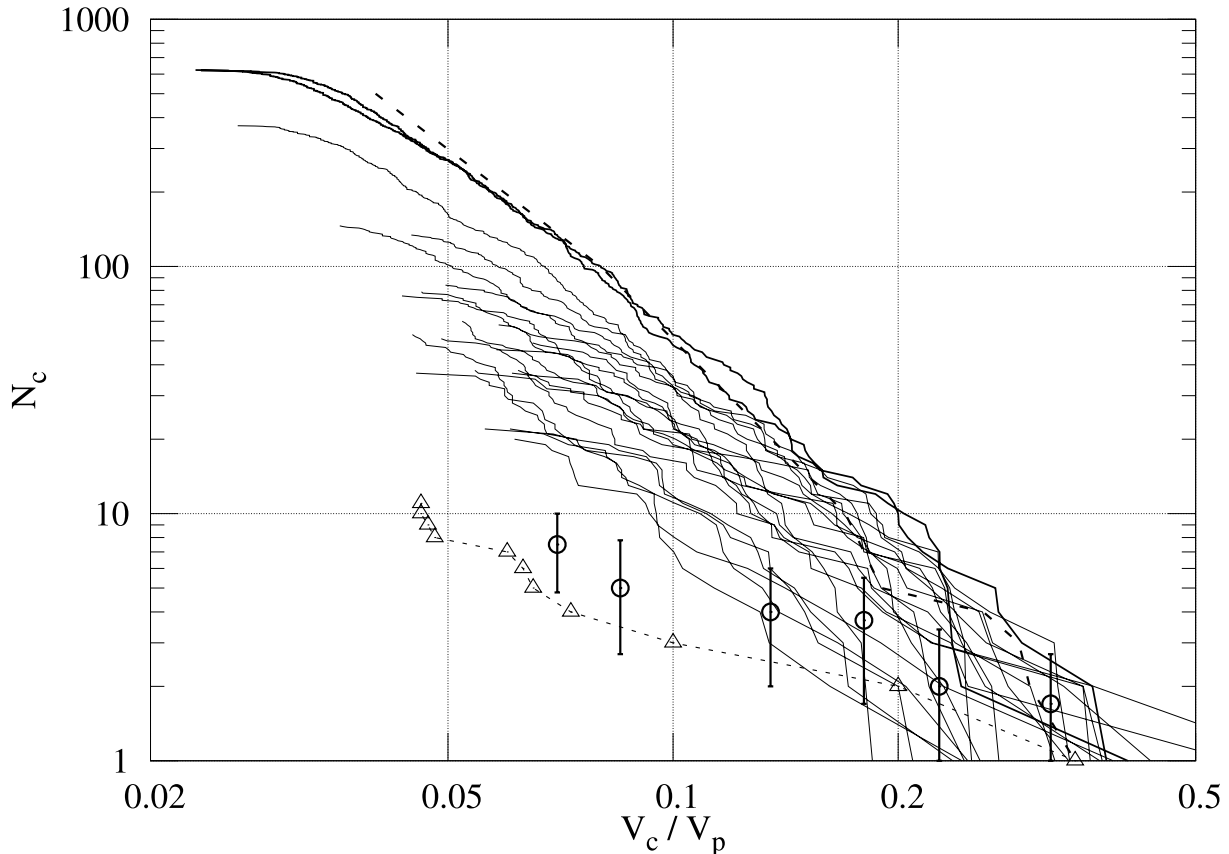


Fig. 2. Cumulative numbers of subhalos as a function of their maximum circular velocities v_c normalized by those of the parent halos v_p for all 21 selected halos. Two upper bold curves are for those of group-sized halos G1 and G2. The thick dashed curve is the result of Moore et al. (1999) for a galaxy-sized halo. The thin dashed curve with open triangles denotes the dwarf galaxies in our galaxy (Mateo 1998). Open circles with error bar show the dwarf galaxies in the local group (D’Onghia et al. 2007).

(Pentium 4/2.8GHz, i865) each of which has one GRAPE-6A board. The simulation presented below needs ~ 280 seconds per timestep, and thus one run (4930 timesteps) is completed in 380 hours (wallclock time).

In Table 1, we summarize the mass M , the radius r_v , the maximum rotation velocity, v_p , the total number of particles, N , and the number of particles in the $N_{>0.1}$ -th subhalo, $N_{\text{sub},0.1}$, of the 21 selected halos. We also summarize the three dimensional position ($X/L, Y/L, Z/L$) of the halos in the simulation box, where we set the origin of coordinate at the bottom-left corner of figure 1.

In order to investigate the effect of mass and spatial resolution on the subhalo abundance, we performed one simulation in which several subhalos are replaced with higher-resolution ones. We selected two subhalo-poor halos (G16 and G20) and one subhalo-rich one (G18). We picked particles within $5r_v$ from the center of these halos at $z=0$, and traced these particles back to the initial condition. We replaced these particles with higher-resolution particles ($3.7 \times 10^5 M_\odot$), and re-ran the simulation. The total number of timesteps was 9869. The gravitational softening we used was constant in the comoving coordinates for $z > 10$, and was constant (0.89 kpc) in the physical coordinates for $z < 10$. We labeled these halos HG16, HG18, HG20. In the bottom of Table 1, we summarize the prop-

erties of these halos.

3. Result

Figure 1 shows the particle distribution in the simulation box at $z = 0$. The length of the side L is 21.4 Mpc. We unbiasedly selected 21 (parent) halos for which the maximum rotation velocity exceeds 200km/s. The rotation velocity is defined as $v_{\text{cir}}(r) = \sqrt{GM(r)/r}$.

Figure 2 shows the cumulative distribution of subhalos as the function of circular velocities for the selected 21 halos together. We identify all local potential minima within the virial radius r_v as subhalos. In Figure 2, we plot cumulative numbers of subhalos as a function of their maxima of circular velocity, v_c , scaled by those of the parent halos v_p . Two upper bold curves indicate those of group-sized (more than $10^{13} M_\odot$) halos, G1 and G2. Other thin solid curves are for other 19 less massive halos. We can see that the number of subhalos in these halos shows very large variation. The thick dashed curve is the result of Moore et al. (1999a) for a galaxy-sized halo. Moore et al.’s halo has the similar number of subhalos as that of the most subhalo-rich halos in our simulation. Thin curve with open triangles denotes the dwarf galaxies in our galaxy (Mateo 1998). The distribution of

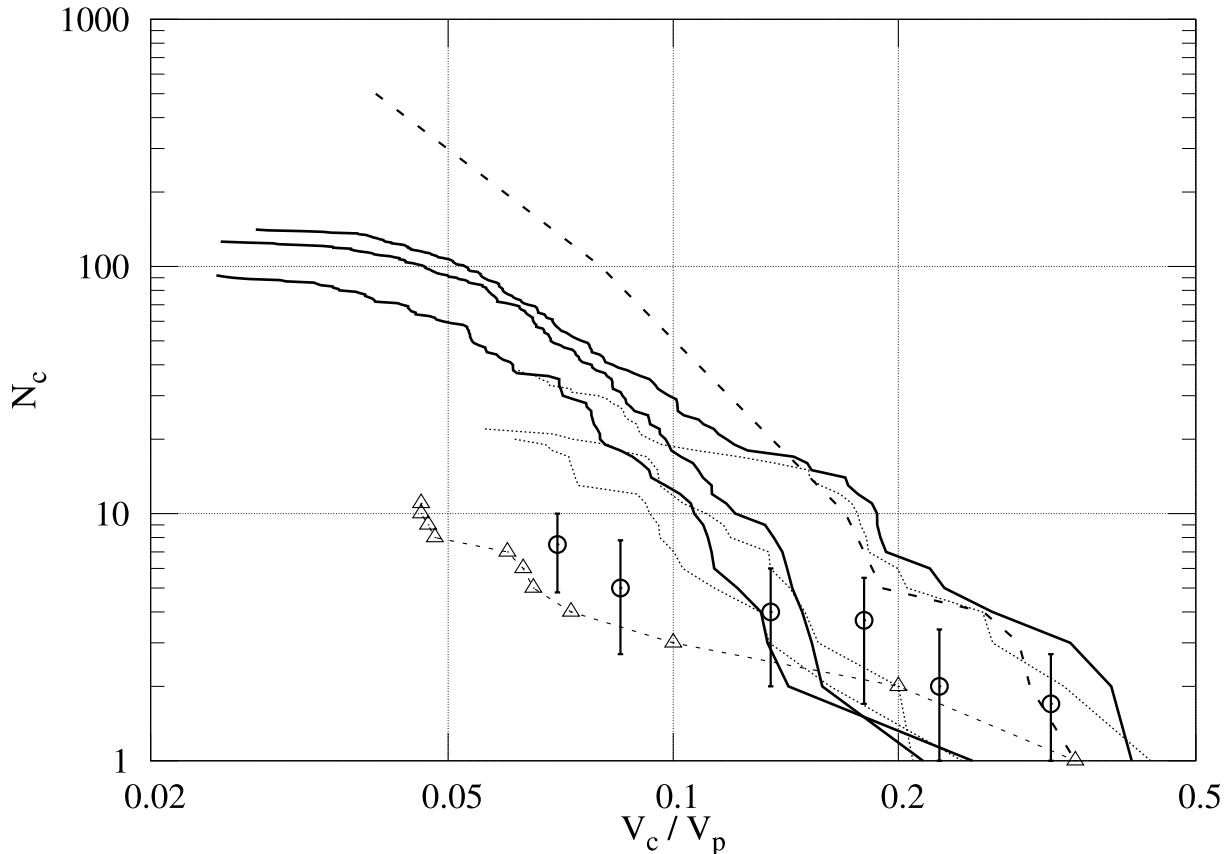


Fig. 3. Same as figure 1 for two subhalo-poor halos G16, G20 and a subhalo-rich one G18. Thick curves are the results of the higher resolution simulation. Thin dotted curves are the results of the original simulation. From top down, the results of G18, G20, G16 are plotted. The thick dashed curve is the result of Moore et al. (1999) for a galaxy-sized halo. The thin dashed curve with open triangles denotes the dwarf galaxies in our galaxy (Mateo 1998). Open circles with error bar show the dwarf galaxies in the local group (D’Onghia et al. 2007).

dwarf galaxies in our galaxy is not too different from that of the most subhalo-poor halos in our simulation. Open circles with error bar show the dwarf galaxies in the local group (D’Onghia et al. (2007), who gave somewhat larger number of dwarfs than Mateo (1998) did). We can see that the difference between observation of local group and least subhalo-poor halos in our simulation is pretty small.

Figure 3 shows the velocity distribution function of subhalos for three selected halos (G16, G18 and G20) together. Thick curves are the results of the higher resolution simulation. Thin dotted curves are the results of the original simulation. From top down, the results of G18, G20, G16 are plotted. The number of subhalos is larger for the higher resolution simulation, in particular for small subhalos. The number of subhalos with $v_c/v_p > 0.1$ in high-resolution runs is about 1.6 times larger than that in the original simulation, for all three subhalos. Thus, large variation in the number of subhalo is also visible in high-resolution run, and it is not a numerical artifact. On the other hand, the original simulation gives systematically low number of subhalos at least for these halos with small total mass. This means that we must correct the number of subhalos in original simulation. In order to make a correction to the result of the original simulation using

the higher resolution simulation, we apply the following correction formula

$$N_{>0.1, \text{corrected}} = C N_{>0.1, \text{original}}, \quad (1)$$

$$C = \begin{cases} 1.6 & V_p < 200 \text{ km/s} \\ 1 - 0.6 \log_2(V_p/400) & 200 < V_p < 400 \\ 1 & V_p > 400 \end{cases} \quad (2)$$

where $N_{>0.1}$ is the number of subhalos with circular velocity more than 10% of that of the parent halo. We use this corrected number as the measure of the subhalo abundance. We used this measure because it is known to be safe against small- N effects. Number counts for subhalos containing less than 200 particles is not reliable (Kase et al. 2007). Even for G21, the subhalos with $v_c/v_p > 0.1$ contain more than 200 particles. The systematic difference we found is probably due to the rather large softening used in the original simulation.

In order to understand the origin of this large variation in the subhalo abundance, we investigated the dependence of the abundance on various quantities. Figure 4 shows the result. The subhalo abundance clearly depends on the mass of the parent halo, as seen in figure 4a. However, if we consider only galaxy-sized halos (halo mass less than $5 \times 10^{12} M_\odot$), there remains very large scatter in the abun-

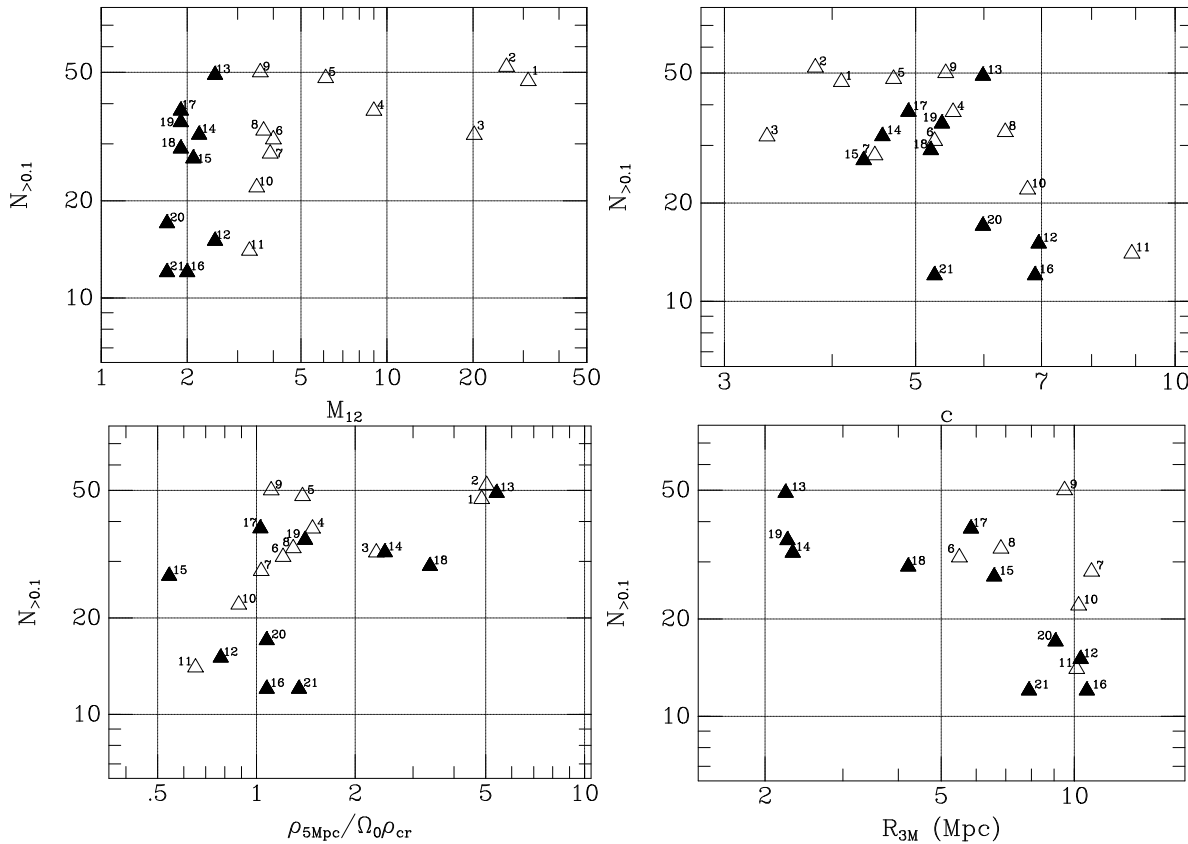


Fig. 4. Dependence of subhalo abundance $N_{>0.1}$ on (a) mass M_{12} in unit of $10^{12}M_{\odot}$ (upper-left), (b) concentration parameter $c = r_0/r_v$ (upper-right), (c) local density within 5Mpc (lower-left), and (d) distance to influential larger-sized halos, R_{3M} , of parent halos (lower-right). The numbers near symbols indicate the halo IDs. The black triangle symbols mean the halos of $M < 3 \times 10^{12}M_{\odot}$.

dance. Massive halos (mass $M > 5 \times 10^{12}M_{\odot}$) are all abundant in subhalos.

Figure 4b shows the dependence on the concentration parameter $c = r_0/r_v$, where r_0 is the break radius for the fit to Moore et al.’s profile (Moore et al. 1999b) and r_v is again the virial radius. More centrally-concentrated halos have fewer subhalos. This dependence might mean that the concentrated halos, which are dynamically more evolved, have fewer subhalos.

Figure 4c shows the dependence on the local mass density averaged over 5Mpc. Again, there is clear correlation, and if the parent halo is in a low density region, it contains less subhalos, though some of low-mass halos in low-density region (G15, G17 and G19) have relatively many halos.

Figure 4d shows the dependence on the distance to the nearest halo with mass more than three times the mass of the parent halo. This is another way to measure the effect of the environment. The dependence is similar to that on the local density, but we can see that halos G17 and G19, which are in low-density regions but relatively rich in subhalos, have nearby massive halos. From figures 4c and 4d, we can conclude that galaxy-sized halos have small number of subhalos if they are formed in low-density region, with no nearby massive halos.

This dependence on the local environment is somewhat counter-intuitive. No matter what the external environ-

ment is, halos should be formed bottom-up, and the merging history, which might have some effect on the subhalo abundance, should not depend much on the local density *outside* the halo, as far as the mass and velocity dispersion of the halos are similar. As we can see from table 1, velocity dispersion depends strongly on the halo mass and therefore dependence on the local density is weak.

Figure 5 shows one subhalo-poor halo (G16) and one subhalo-rich one (G18) at $z = 0$ and $z = 3$. For $z = 3$, only particles which is in the halo’s virial radius at $z = 0$ are plotted. From panels for $z = 0$, we can clearly see the large difference in the subhalo abundance. From panels for $z = 3$, we can see that they have very different shapes. Subhalo-poor halos are much more centrally concentrated than subhalo-rich ones. Thus, even though they initially contain large number of substructures, many of them are disrupted or lost most of mass due to the tidal field of the parent halo. On the other hand, subhalo-rich halos have many substructures which are distant from the high-density central region of the parent halo, and many of them survived to $z = 0$, simply because they remain far away from the high-density region of the parent halo.

The difference in the shape at $z = 3$ is the direct consequence of the difference in the local density. The regions which will become galaxy-sized halo have similar average density at early time, whether or not they are in the high-density region or low-density region. However, this means

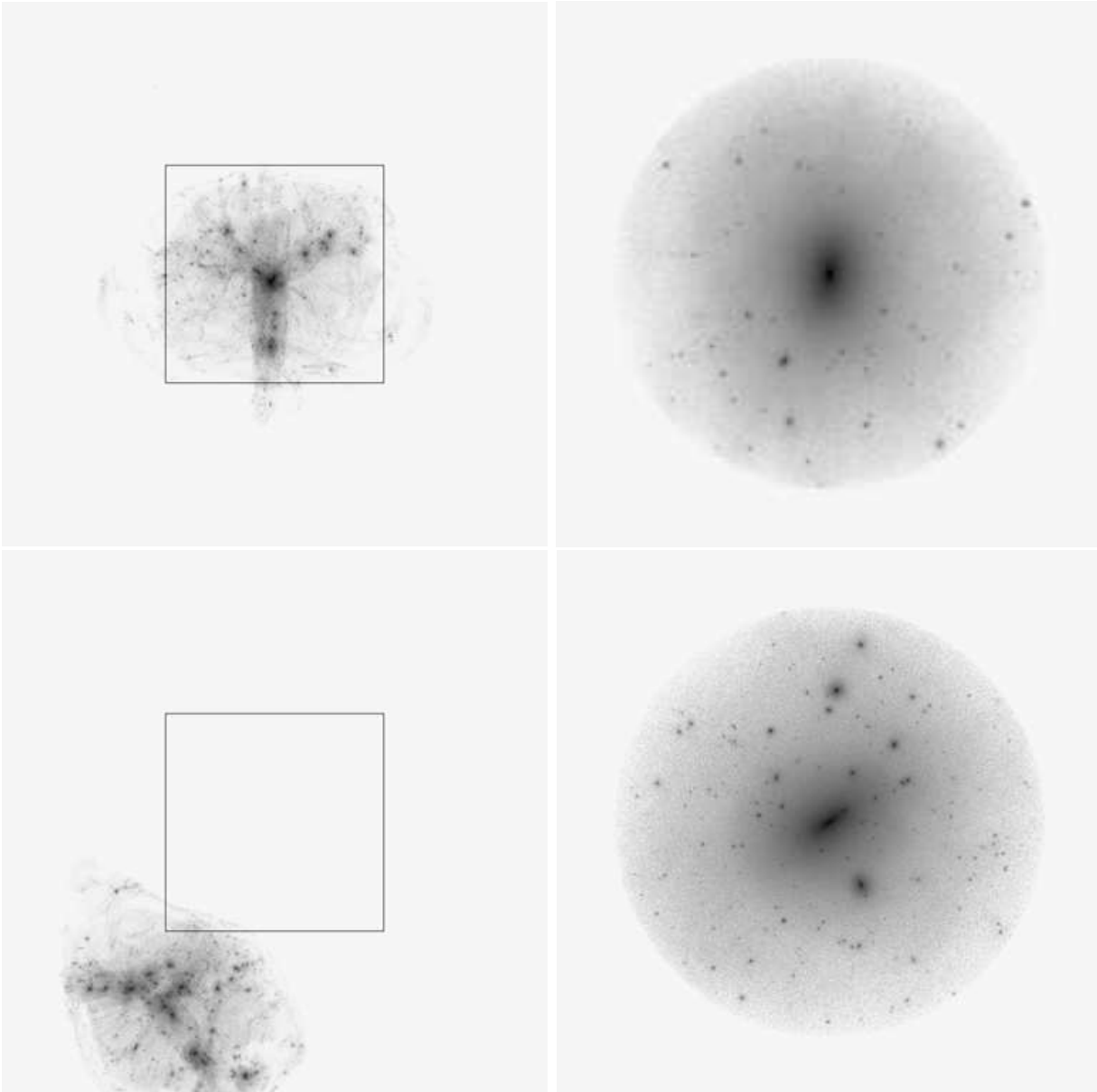


Fig. 5. Snapshots of a subhalo-poor halo G16 and a subhalo-rich one G18 (upper to lower) at $z=3$ (left) and $z=0$ (right). The width is 2Mpc (left) and 0.8Mpc (right). The boxes on the left snapshots show the regions of the right snapshots.

that halos in the low-density region must have more power in the small-scale density fluctuation which directly corresponds to the halo mass, since they do not have the contribution of large-scale fluctuations. Thus, they are more centrally concentrated. As we have seen above, the concentration shows as anti-correlation with the subhalo abundance.

Another possible effect is the difference in the external tidal field. From figure 5, we can see that halos G16 did not move much from $z = 3$ to $z = 0$, while G18 traveled a rather large distance. This difference is because of the difference in the external tidal field. The external tidal field has the effect of changing the orbits of subhalos, generally adding more angular momenta. Thus, subhalos in the halos in high-density regions have orbits with larger

pericenter distances.

In the case of cluster-sized or even group-sized halos, this effect of the local environment must be relatively weak, because the density fluctuations with mass scale larger than the cluster mass do not have much power. Thus, this strong environmental effect is unique to the galaxy-sized halos. The reason why this effect is overlooked in previous studies is, in our opinion, the prejudice that the gravitational structure formation is scale free and dark halos should behave in the same way irrespective of their masses or environments.

4. Conclusion

We have performed the simulation of a single large volume and measured the abundance of subhalos in all massive halos. We found that the variation of the subhalo abundance is very large. The subhalo abundance depends strongly on the local density of the background. Halos in high-density regions contain large number of subhalos. Our galaxy is in the low-density region. For our simulated halos in low-density regions, the number of subhalos is within a factor of four to those of our galaxy or local group.

We conclude that the “missing dwarf problem” was to a large extent caused by the biases introduced in the standard practice used to prepare initial conditions for cosmological simulations, and if we construct unbiased samples, galaxy-sized halos in low-density field region contain subhalos whose number is not inconsistent with the number of dwarf galaxies in the Local group.

We are grateful to Kohji Yoshikawa for providing his parallel TreePM code. We thank Hiroyuki Kase and Keigo Nitadori for their technical advices and helpful discussions. Numerical computations were in part carried out on the PC cluster at Center for Computational Astrophysics (CfCA), National Astronomical Observatory of Japan. This research is partially supported by the Special Coordination Fund for Promoting Science and Technology (GRAPE-DR project), Ministry of Education, Culture, Sports, Science and Technology, Japan.

References

- Bertschinger, E. 1995, ArXiv Astrophysics e-prints, arXiv:astro-ph/9506070
- D’Onghia, E., Maccio’, A. V., Lake, G., Stadel, J., & Moore, B. 2007, ArXiv e-prints, 704, arXiv:0704.2604
- Fukushige, T., Makino, J., Kawai, A., 2005, PASJ, 57, 1009
- Kamionkowski, M., and Liddle, A. R., 2000, Phys. Rev. Lett., 84, 4525
- Kase, H, Funato Y., and Makino J., 2007, PASJ, in press
- Klypin, A, Kravtsov, A. V., Valenzuela, O., Prada, F., 1999, ApJ, 522, 82
- Kravtsov, A. V., Gnedin, O. Y., Klypin, A. A., 2004, ApJ, 609, 482
- Mateo, M. L., 1998, ARA&A, 36, 435
- Moore, B., Ghigna, S., Governato, F., Lake, G., Quinn, T., Stadel, J., Tozzi, P., 1999a, ApJ, 524, L19
- Moore, B., Quinn, T., Governato, F., Stadel, J., Lake, G., 1999b, MNRAS, 310, 1147
- Spergel, D. N., and Steinhardt, P. J., 2000, Phys. Rev. Lett., 84, 3760
- Stoehr, F., White, S. D. M., Tormen, G., Springel, V., 2002, MNRAS, 335, L84
- Sugimoto, D., Chikada, Y., Makino, J., Ito, T., Ebisuzaki, T., 1990, Nature, 345, 33
- Susa, H., and Umemura, M., 2004, ApJ, 610, L5
- Yoshikawa, K., and Fukushige T., 2005, PASJ, 57, 849

Table 1. Selected Halos

Halo ID	M ($10^{12}M_{\odot}$)	r_v (kpc)	V_p (km/s)	N	$N_{\text{sub},0.1}$	X/L	Y/L	Z/L
G1	31.2	798	472	10466465	2241	0.454	0.687	0.637
G2	26.2	752	421	8780560	1969	0.394	0.694	0.701
G3	20.0	688	434	6700220	1625	0.793	0.776	0.475
G4	9.0	528	334	3025883	993	0.291	0.761	0.960
G5	6.1	465	284	2063080	527	0.126	0.969	0.363
G6	4.0	404	258	1355302	423	0.159	0.677	0.597
G7	3.9	398	250	1299438	373	0.273	0.169	0.556
G8	3.7	393	251	1251621	404	0.516	0.482	0.905
G9	3.6	389	247	1214417	343	0.672	0.775	0.037
G10	3.5	386	260	1180493	417	0.933	0.380	0.704
G11	3.3	379	278	1115028	496	0.691	0.343	0.312
G12	2.5	343	244	830204	390	0.484	0.234	0.815
G13	2.5	343	219	828903	242	0.364	0.712	0.799
G14	2.2	329	211	737135	230	0.898	0.778	0.446
G15	2.1	324	205	701198	224	0.340	0.058	0.897
G16	2.0	317	227	655852	323	0.921	0.269	0.705
G17	1.9	317	202	653996	202	0.968	0.131	0.514
G18	1.9	316	202	650187	208	0.230	0.594	0.658
G19	1.9	313	200	626605	217	0.183	0.951	0.449
G20	1.7	305	200	584875	214	0.777	0.836	0.894
G21	1.7	301	200	559250	221	0.505	0.381	0.861
HG16	1.9	315	228	5189215	1715	0.921	0.269	0.706
HG18	1.9	314	203	5140043	1308	0.228	0.592	0.658
HG20	1.7	303	200	4666533	1357	0.778	0.836	0.895